

# Review of Computer Engineering Research

2023 Vol. 10, No. 2, pp. 40-54

ISSN(e): 2410-9142

ISSN(p): 2412-4281

DOI: 10.18488/76.v10i2.3471

© 2023 Conscientia Beam. All Rights Reserved.



## Bias field correction-based active contour model for region of interest extraction in digital image

 Nurul Ain Suraya Rosli<sup>1</sup>

 Abdul Kadir Jumaat<sup>1,2\*</sup>

 Mohd Azdi Maasar<sup>3</sup>

 Mohamed Faris Laham<sup>4</sup>

 Normahirah Nek Abd Rahman<sup>5</sup>

<sup>1</sup>Department of Mathematics, Faculty of Computer and Mathematical Sciences, Universiti Teknologi MARA, 40450, Shah Alam, Selangor, Malaysia.

<sup>1,2</sup>Institute for Big Data Analytics and Artificial Intelligence, Universiti Teknologi MARA, 40450, Shah Alam, Selangor, Malaysia.

<sup>1</sup>Email: [nurulainsurayarosli23@gmail.com](mailto:nurulainsurayarosli23@gmail.com)

<sup>2</sup>Email: [abdulkadir@tmsk.uitm.edu.my](mailto:abdulkadir@tmsk.uitm.edu.my)

<sup>3</sup>School of Mathematical Sciences, College of Computing, Informatics and Media, Universiti Teknologi MARA Negeri Sembilan Branch, Seremban Campus, Malaysia.

<sup>3</sup>Email: [azdimaasar@tmsk.uitm.edu.my](mailto:azdimaasar@tmsk.uitm.edu.my)

<sup>4</sup>Institute for Mathematical Research, Universiti Putra Malaysia, Malaysia.

<sup>4</sup>Email: [mohdfaris@upm.edu.my](mailto:mohdfaris@upm.edu.my)

<sup>5</sup>Pusat GENIUS@Pintar Negara, Universiti Kebangsaan Malaysia, UKM Bangi, Selangor, Malaysia.

<sup>5</sup>Email: [normahirah@ukm.edu.my](mailto:normahirah@ukm.edu.my)



(+ Corresponding author)

### ABSTRACT

#### Article History

Received: 20 June 2023

Revised: 18 August 2023

Accepted: 25 August 2023

Published: 15 September 2023

#### Keywords

Active contours

Bias correction

Intensity inhomogeneity

Level set

Selective image segmentation.

The region-based Active Contour Model (ACM) is a widely known variational segmentation model for extracting or segmenting a digital image into numerous sections for further analysis. Distinguishing between global and specific segmentation models within this paradigm is possible. The global segmentation model is incapable of selectively segmenting the region of interest (ROI) from the input image, which leads to an over-segmented problem. A variety of models have been devised to address the task of selective segmentation, which involves the extraction of the boundary of a particular region of interest (ROI) inside a digital image. The Primal Dual Selective Segmentation (PDSS) model has been recently introduced and exhibits significant potential in terms of accuracy. Nevertheless, the presence of intensity inhomogeneity in digital images disrupts the precision and localisation of target regions of segmentation. Therefore, it is important to take into account bias field adjustment, also known as correction for intensity inhomogeneity. So, this study came up with a new selective segmentation model called the Selective Segmentation with Bias Field Correction (SSBF) model by combining the idea of the existing PDSS model with the level set-based bias field correction technique. To solve the proposed SSBF model, we first derived the Euler-Lagrange (EL) equation and solved it in MATLAB software. The Intersection over Union (IOU) coefficient, also known as the Dice (DSC) and Jaccard (JSC) similarity metrics, evaluated the proposed model's accuracy. Experimental results demonstrate that the JSC and DSC values of the proposed model were 13.4% and 7.2% higher, respectively, than the competing model.

**Contribution/Originality:** By combining the level set-based bias field idea with the primal dual selective segmentation idea, a new ACM is made that can effectively find the edge of the ROI in digital images with different intensities. Various digital images from different sources were used to implement the new model.

## 1. INTRODUCTION

Digital image boundary extraction, also known as picture segmentation, refers to the process of dividing a specific region of interest (ROI) inside a digital image into multiple distinct portions [1]. Pixels in each region have similar features, such as intensity, colour, texture, or other attributes, which are vital in computer vision applications including object detection, image fusion, and image retrieval [2-6]. The image is simplified so that meaningful information can be extracted for subsequent research.

There are two distinct categories of segmentation methods: deep learning-based approaches and model-based approaches [2]. Learning-based approaches use deep neural networks to derive semantic information that is portioned to each pixel to achieve segmentation. However, apart from its satisfactory performance, large requirements for data volume (including the label data), storage space, and running time will limit its practical applications [2]. The edge-based method and region-based approaches are examples of model-based methods that are capable of complementing the learning-based methods. These models are less dependent on the amount of data and require no label or ground truth data. Intensity discontinuities in transitional image structure, such as edges, are used in edge-based approaches to separate objects from the backdrop. The edge detectors are illustrations of edge-based techniques that identify object and background regions by calculating the gradient of each pixel. The edge-based approach is vulnerable to picture noise [7]. The primary emphasis of region-based techniques is the image region's statistical feature homogeneity. Segmentation is carried out using the homogeneity difference between the object and background zones. It performs better for images with weak boundaries and has a lower noise sensitivity. The region-based technique may establish image boundaries that are far from the original segmentation contour and is less impacted by where the original segmentation contour is located. The boundary of an ROI may be successfully extracted from a digital image using the well-known region-based technique known as active contour model (ACM). One of the most well-known region-based models is the ACM model, specifically the Chan-Vese (C-V) model [8], which is based on the Mumford-Shah functional in Mumford and Shah [9].

The techniques discussed above are global-type segmentation strategies that can be employed to obtain feature segmentation for all characteristics. However, it is not possible to use them for the purpose of segmenting a particular object from an image. The selective image segmentation model, a different kind of image segmentation, is needed for this purpose. The Convex Distance Selective Segmentation (CDSS) model and the Primal Dual Selective Segmentation (PDSS) model are two efficient selective ACMs that have been created [10, 11]. The Mumford-Shah function served as the foundation for the creation of the CDSS model, which is used to segment grayscale pictures. Meanwhile, segmentation computation time is efficiently produced using the PDSS model, a reformed version of the CDSS model. But segmenting a targeted item in pictures with intensity inhomogeneity is not the PDSS model's intended use. Intensity inhomogeneity is noticeable in contemporary photos due to variables such as spatial fluctuations in lighting and imaging equipment abnormalities, which present various problems in image processing and computer vision [12]. In digital imaging, poor picture capture frequently results in intensity inhomogeneity. For instance, a non-uniform field or a non-uniform sensitivity of the receiver and transmitter coils can cause inhomogeneities in radio frequency fields. These distortions caused the same item types' intensities to vary across the picture, which was undesirable. Therefore, efficient and reliable methods of addressing intensity inhomogeneity are required [13].

In order to address the issue of intensity inhomogeneity, researchers [12] considered the local picture intensity information, which is then outlined as the following Equation 1:

$$U = f \cdot I + n \quad (1)$$

Here, the measured image is denoted by  $U$ ,  $I$  is the actual image,  $f$  is the component of intensity inhomogeneity, and  $n$  is the component of noise. A component  $f$  is also known as a bias field or a shading picture. The actual image  $I$  is used to quantify an intrinsic, roughly constant physical property of the objects that is thought to be piecewise constant. It is assumed that the bias field  $f$  varies gradually. One can suppose that the additive noise  $n$  is zero-mean

Gaussian noise. The difficulty in segmenting pictures with intensity inhomogeneity is specifically due to the overlapping throughout the range of intensities in the region of interest.

Based on Equation 1, researchers [12] made the Level Set Based Bias Field Correction (LSBF) model, which is a local intensity clustering ACM, to deal with the uneven intensity. This model determines and specifies the local clustering intensity, which is subsequently integrated with regard to the neighbourhood centre. As a global form of ACM, the LSBF model may not be able to selectively segment a specific item in an image, even though it is excellent at segmenting pictures with intensity inhomogeneity.

Therefore, by using the concepts from the PDSS model and the LSBF model, this study will develop a new selective kind of ACM termed the Selective Segmentation with Bias Field Correction (SSBF) model. The LSBF and PDSS models will be reviewed in the next section, and then the suggested SSBF model will be presented and its solution will be covered. The final section establishes our conclusion and the recommendations for further research after the numerical experiments are shown.

## 2. REVIEW OF RELATED MODELS

In Section 2, we'll look at two important models to help us come up with a new selective ACM for finding the edges of ROI in digital images with different intensities. The LSBF model is the first, followed by the PDSS model.

### 2.1. Level Set Based Bias Field Correction (LSBF) Model

Li, et al. [12] suggested a new region-based image segmentation method that can handle intensity inhomogeneities in the segmentation. The local clustering criterion function for the intensities in each point's neighbourhood is defined as a result when the local intensity clustering property is derived. The neighbourhood centre is used to define an energy functional, which is then transformed into a level-set formulation. The level-set function is depicted as a partition of the image domain and a bias field that compensates for the intensity inhomogeneity. Let the segmentation contour be represented by the zero-level set function  $\phi$  which is used to indicate the two regions  $\Omega_1$  and  $\Omega_2$  of image domain  $\Omega = (x, y)$ . Assumes that  $N_1(\phi) = H(\phi)$  and  $N_2(\phi) = 1 - H(\phi)$  are the functions that defined with the regions, where  $H$  is the Heaviside function and  $U(x)$  is the input image. Then, a truncated Gaussian function  $G(y - x)$  is defined to compute local intensity clustering. To smooth the segmentation contour, a function  $\nabla H(\phi)$  is defined and to ensure stability of  $\phi$ , the potential function  $(1/2)(|\nabla\phi| - 1)^2$  is introduced. Thus, the energy function of the LSBF model is then defined by the following Equation 2:

$$\begin{aligned} \varepsilon(\phi, k, f) = & \int (\sum_{i=1}^N \int G(y - x) |U(x) - f(y)k_i|^2 N_i(\phi(x)) dx) dy \\ & + \int \nabla H(\phi) dx dy + \int (1/2)(|\nabla\phi| - 1)^2 dx dy \end{aligned} \quad (2)$$

Where  $k_i = k_1, k_2, \dots, k_N$  is a constant and represented as vector  $k$  and  $f$  is the bias field. The Equation 2 is minimized iteratively using a gradient descent approach. The LSBF was invented for segmenting whole objects, which is inapplicable in the case of selective segmentation.

### 2.2. Primal Dual Selective Segmentation (PDSS) Model

Jumaat and Chen [11] proposed a new minimization problem in the primal-dual framework, termed the Primal Dual Selective Segmentation (PDSS) model, allowing them to obtain a fast solution. The model is expressed as the following Equation 3:

$$\begin{aligned} \min_{u,w} J(u, w) = & \mu \int_{\Omega} |\nabla u|_g d\Omega + \int_{\Omega} rwd\Omega + \theta \int_{\Omega} P_d w d\Omega \\ & + \alpha \int_{\Omega} v(w) d\Omega + \frac{1}{2\rho} \int_{\Omega} (u - w)^2 d\Omega \end{aligned} \quad (3)$$

Based on Equation 3, the first term weighted by  $\mu > 0$  is used to smooth the segmentation curve. The second integrand is the image-fitting term with  $w$  as the new and dual variable. The term  $P_d$  is the distance fitting term, weighted by  $\theta > 0$ . The second and the third terms are used to capture the boundaries of the targeted ROI. The fourth term weighted by  $\alpha > 0$  is used to ensure the solution  $u \in [0,1]$  and the last integrand weighted by  $\rho > 0$  ensures  $u \approx w$ . In alternating minimization form, it is correspond to solving the following Equations 4 and 5:

$$\min_u J_1(u, w) = \mu \int_{\Omega} |\nabla u|_g d\Omega + \frac{1}{2\rho} \int_{\Omega} (u - w)^2 d\Omega, \tag{4}$$

$$\min_{w \in (0,1)} J_2(u, w) = \int_{\Omega} r w d\Omega + \theta \int_{\Omega} P_d w d\Omega + \frac{1}{2\rho} \int_{\Omega} (u - w)^2 d\Omega \tag{5}$$

In Equation 4, the highly computational term  $v(w)$  is dropped, while Equation 5 will produce an analytical solution. Consequently, the model is less complex and less sensitive to parameter choices.

While this model is capable of selectively segmenting a particular ROI, the PDSS model may deliver unsatisfactory results in segmenting images with intensity inhomogeneity. This is mainly because the model assumes that the input image is homogeneous. Hence, in this study, the new proposed SSBF model is formulated to solve the drawbacks of the existing models.

### 3. THE PROPOSED MODEL

The idea of the formulation is on images  $U = U(x, y)$ , there is  $n_1 (\geq 3)$  geometrical points  $C$  located near to the boundary of the image and construct an initial polygon  $P$ . The marker set  $C$  is defined as the following Equation 6:

$$C = \{w_i = (x_i^*, y_i^*) \in \Omega, 1 \leq i \leq n_1\} \subseteq \Omega \tag{6}$$

Following from the marker set, function  $P_d(x, y)$  is defined as the Euclidean distance of each point  $(x, y) \in \Omega$  from its nearest points of  $(x_p, y_p) \in P$ , defined as the following Equation 7:

$$P_d(x, y) = \sqrt{(x - x_p)^2 + (y - y_p)^2} \tag{7}$$

Thus, by utilizing all the ingredients and integrating the LSBF model with PDSS model, the proposed SSBF model is defined as the following Equation 8:

$$\begin{aligned} SSBF(\phi, k, f) = & \int_{\Omega} \left( \sum_{i=1}^2 \int_{\Omega} G(y - x) |U(x) - f(y)k_i|^2 N_i(\phi(x)) dx \right) dy + \beta \int_{\Omega} \delta(\phi) |\nabla \phi| dx dy \\ & + \mu \int_{\Omega} \frac{1}{2} (|\nabla \phi| - 1)^2 dx dy + \theta \int_{\Omega} P_d H_{\varepsilon}(\phi) dx dy \end{aligned} \tag{8}$$

Where  $G = e^{-\frac{(x-y)^2}{2\sigma^2}}$  while  $\mu$  and  $\beta$  are fixed parameter for the regularizing term and length term respectively.

Additionally,  $H_{\varepsilon}(\phi)$  in Equation 8 is the smoothed Heaviside function where  $\varepsilon$  is a positive number and expressed as the following Equation 9:

$$H_{\varepsilon}(\phi) = \frac{1}{2} \left[ 1 + \frac{2}{\pi} \arctan \left( \frac{\phi}{\varepsilon} \right) \right] \tag{9}$$

The function  $N_i(\phi(x))$  in Equation 8 represented the membership function of the regions  $\Omega_i (i = 1,2)$ , defined by the following Equation 10:

$$\begin{cases} N_1(\phi(x)) = H_{\varepsilon}(\phi(x)), \\ N_2(\phi(x)) = 1 - H_{\varepsilon}(\phi(x)). \end{cases} \tag{10}$$

The solution of the SSBF model in Equation 8 is obtained by minimizing the energy. The energy minimization is achieved by an iterative process: in each iteration, the minimization of the energy  $SSBF(\phi, k, f)$  is done with respect to each of its variable  $\phi, k$  and  $f$ . We provide the solution to the energy minimization with respect to each variable as follows.

1. Energy minimization with respect to  $\phi$  : For fixed  $k$  and  $f$ , the minimization of  $SSBF(\phi, k, f)$  in Equation 8 with respect to  $\phi$  can be achieved by solving its Euler Lagrange (EL) equation using gradient descent

method. To derive the EL equation, let the integrands denoted by  $I_1(\phi) = G(y - x)|U(x) - f(y)k_1|^2 H_\epsilon(\phi)$ ,  $I_2(\phi) = G(y - x)|U(x) - f(y)k_2|^2 (1 - H_\epsilon(\phi))$ ,  $I_3(\phi) = \delta(\phi)|\nabla\phi|$ ,  $I_4(\phi) = 0.5(|\nabla\phi| - 1)^2$  and  $I_5(\phi) = P_d H_\epsilon(\phi)$  where  $k$  and  $f$  are fixed. Note that we will demonstrate on the derivation of EL equation for the  $I_1$  only because the working steps to derive the EL equations for  $I_2 \dots I_5$  are similar.

Next, additional term  $\bar{\epsilon}v$  is added at the level set function  $\phi$  such that  $\phi = \phi + \bar{\epsilon}v$  where  $v$  is an arbitrary test function and  $\bar{\epsilon}$  is a real parameter close to 0. Clearly,

$$I_1(\phi + \bar{\epsilon}v) = G(y - x)|U(x) - f(y)k_1|^2 H_\epsilon(\phi + \bar{\epsilon}v)$$

Then, we differentiate  $I_1(\phi + \bar{\epsilon}v)$  with respect to  $\bar{\epsilon}$  that yield the following Equation 11:

$$\frac{d}{d\bar{\epsilon}} I_1(\phi + \bar{\epsilon}v) = G(y - x)|U(x) - f(y)k_1|^2 \delta_\epsilon(\phi + \bar{\epsilon}v)v \tag{11}$$

By applying the Taylor expansion at  $\bar{\epsilon} = 0$ ;

$$\begin{aligned} I_1(\phi + \bar{\epsilon}v) &= I_1(0) + I_1(0)\bar{\epsilon} + O(\bar{\epsilon}^2) \\ &= G(y - x)|U(x) - f(y)k_1|^2 H_\epsilon(\phi) + G(y - x)|U(x) - f(y)k_1|^2 \delta_\epsilon(\phi)v\bar{\epsilon} \\ &\quad + O(\bar{\epsilon}^2) \end{aligned}$$

Now, we compute the first variation of  $I_1(\phi)$  with any  $v$  and simplified the equation into the following Equation 12:

$$\begin{aligned} &\int_{\Omega} \frac{I_1(\phi + \bar{\epsilon}v) - I_1(\phi)}{\bar{\epsilon}} dx dy \\ &= \frac{1}{\bar{\epsilon}} \int_{\Omega} [G(y - x)|U(x) - f(y)k_1|^2 \delta_\epsilon(\phi)v\bar{\epsilon} + O(\bar{\epsilon}^2)] dx dy \end{aligned} \tag{12}$$

Consequently, for any function of  $v$ , we have computed the limit using the following Equation 13:

$$\lim_{\bar{\epsilon} \rightarrow 0} \frac{I_1(\phi + \bar{\epsilon}v) - I_1(\phi)}{\bar{\epsilon}} = 0 \tag{13}$$

Thus, the Equation 12 will be transformed as the following Equation 14:

$$\int_{\Omega} [G(y - x)|U(x) - f(y)k_1|^2 \delta_\epsilon(\phi)v] = 0 \tag{14}$$

Factorize  $\delta_\epsilon(\phi)$  and  $v$  in the Equation 14 yield the following Equation 15:

$$\int_{\Omega} \delta_\epsilon(\phi)v [G(y - x)|U(x) - f(y)k_1|^2] dx dy = 0 \tag{15}$$

Hence, the EL equation for the term  $I_1$  is defined as the following Equation 16:

$$\delta_\epsilon(\phi) [G(y - x)|U(x) - f(y)k_1|^2] = 0 \tag{16}$$

Here,  $\delta_\epsilon(\phi)$  denoted as the Dirac function defined as the following Equation 17:

$$\delta_\epsilon(\phi) = \frac{\epsilon}{\pi(\epsilon^2 + \phi^2)} \tag{17}$$

By similar operation, the EL equation for the remaining terms can be computed. Thus, for  $I(\phi) = I_1(\phi) + I_2(\phi) + I_3(\phi) + I_4(\phi) + I_5(\phi)$ , the EL equation for the SSBF model is defined as follows:

$$\delta_\epsilon(\phi) \left[ \begin{aligned} &G(y - x)|U(x) - f(y)k_1|^2 - G(y - x)|U(x) - f(y)k_2|^2 \\ &-\beta\delta(\phi)\nabla \cdot \left(\frac{\nabla\phi}{|\nabla\phi|}\right) - \mu \left(\Delta\phi - \frac{\nabla\phi}{|\nabla\phi|}\right) + \theta Pd \end{aligned} \right] = 0$$

The gradient descent flow is obtained by applying the gradient descent method in the EL equation defined as the following Equation 18:

$$\frac{\partial\phi}{\partial t} = \delta_\epsilon(\phi) \left[ \begin{aligned} &-G(y - x)|U(x) - f(y)k_1|^2 + G(y - x)|U(x) - f(y)k_2|^2 \\ &+\beta\nabla \cdot \left(\frac{\nabla\phi}{|\nabla\phi|}\right) + \mu \left(\Delta\phi - \frac{\nabla\phi}{|\nabla\phi|}\right) - \theta Pd \end{aligned} \right] \tag{18}$$

Where the evolution of  $\phi$  with respect to artificial time  $t$  is represented as  $\frac{\partial\phi}{\partial t}$ .

During the evolution of the level set function according to Equation 18, the constants in  $k$  and the bias field in  $f$  are updated by minimizing the energy  $SSBF(\phi, k, f)$  with respect to  $k$  and  $f$  respectively, which are describe as below.

2. Energy minimization with respect to  $k$  : For fixed  $\phi$  and  $f$ , the optimal  $k$  that minimize the energy  $SSBF(\phi, k, f)$ , denoted by  $\hat{k}_i = (\hat{k}_1, \dots, \hat{k}_N)$  is given by the following Equation 19:

$$\hat{k}_i = \frac{\int U(f * G) N_i(\phi(y))}{\int (f^2 * G) N_i(\phi(y))}, \quad i = 1, 2 \tag{19}$$

3. Energy minimization with respect to  $f$  : For fixed  $\phi$  and  $k$ , the optimal  $f$  that minimize the  $SSBF(\phi, k, f)$ , denoted by  $\hat{f}$  is defined as the following Equation 20:

$$\hat{f} = \frac{(k_i N_i(\phi(y)) U) * G}{(k_i^2 N_i(\phi(y)) * G)} = \frac{(U J^{(1)}) * G}{J^{(2)} * G} \tag{20}$$

Here,  $J^{(1)} = \sum_{i=1}^2 k_i N_i(\phi(y))$  and  $J^{(2)} = \sum_{i=1}^2 k_i^2 N_i(\phi(y))$ . Note that the convolutions with a kernel function  $G$  in Equation 20 proves the slowly varying property of the derived optimal estimator  $\hat{f}$  of the bias field.

The implementation of our proposed model is summarized in Algorithm 1. This algorithm shows the steps involved to implement the SSBF model to compute the solution using MATLAB software.

---

**Algorithm 1:** The SSBF model algorithm

---

1. Set the value of parameters  $\beta$ ,  $\mu$ ,  $\theta$ , and  $\sigma$
  2. Define the marker set  $C$  and determine the distance  $P_d(x, y)$  in Equation 7
  3. Initialize  $\phi^0$ , when  $n = 0$  such that  $\Gamma$  is the boundary of  $P$
  4. Update  $k$  by fixing  $\phi$  and  $f$  in Equation 19
  5. Solve  $\phi$  from the EL equation to obtain  $\phi^{k+1}$  using Equation 18
  6. Update  $f$  by fixing  $\phi$  and  $k$  in Equation 20
  7. If  $\frac{\|\phi^{k+1} - \phi^k\|}{\|\phi^k\|} \leq tol$  or maximum iteration (*maxit*) reached 300 iterations, then stop. Otherwise, return to step 4.  
The tolerance value is set to be  $tol = 0.005$  which is sufficient for curves evolution. Hence, if the result is unsuccessful, return to step 1.
- 

#### 4. EXPERIMENTAL RESULTS

Various experiments were conducted to highlight the strengths and limitations of the proposed model. Firstly, the proposed model, called the SSBF model, was compared with the LSBF model by Li, et al. [12] in dealing with images with intensity inhomogeneity. Then, we also compared our SSBF model with the popular selective segmentation model, which is the IIS model [14]. Next, we compared the SSBF model with the competing PDSS model by Jumaat and Chen [11]. Lastly, parameter sensitivity analysis was performed on the SSBF model, and the limitations of the proposed model were highlighted.

The performance of all models was evaluated by the Dice similarity metric (DSC) and Jaccard similarity metric (JSC), also known as the Intersection over Union (IOU) coefficient, in the range of [0,1] as follows:

$$DSC = \frac{2TP}{(2TP + FP + FN)}, \quad JSC (IOU) = \frac{TP}{TP + FP + FN}$$

Where the values of TP (true positive), FP (false positive), TN (true positive), and FN (false negative) are determined using the following Table 1:

**Table 1.** Confusion matrix for ground truth and segmented images.

| Image type         | Segmented image |    |    |
|--------------------|-----------------|----|----|
|                    | Binary digit    | 1  | 0  |
| Ground truth image | 1               | TP | FN |
|                    | 0               | FP | TN |

According to Table 1, the number of positive categories that are accurately categorized as 1 for both segmented and ground truth pictures with the same pixel value is known as TP (true positive). False positives (FP) are negative categories that are mistakenly labelled as positive in segmented pictures, where the pixel value is always 1. Next, FN (false negative) indicates the segmentation model mistakenly identified the segmented region as a negative category, which is 0, while TN (true negative) indicates the segmentation model correctly identified the negative category [15]. In the following experiments, the dataset with ground truth was provided by Lankton and Tannenbaum [16]; Martin, et al. [17]; Chen [18]; Li, et al. [19]; Moreira, et al. [20]; Rodtook, et al. [21]; Ismahan [22] and Codella, et al. [23].

#### 4.1. Experiment 1: Comparison of the SSBF Model with the LSBF Model

In this experiment, we compared our proposed SSBF model with the LSBF model in order to verify the capability of the SSBF model for selectively segmenting regions of interest. We acknowledge that the initial contour for images used in both models was the same, and the size of the test images was resized to be  $128 \times 128$  pixels. We claimed that the LSBF model is a global segmentation model that is incapable of selectively segmenting a targeted object, which is unfair to compare with our proposed selective segmentation model. However, this experiment was constructed to rectify this claim. We illustrate the outcomes of the segmentation in Figure 1 as follows:

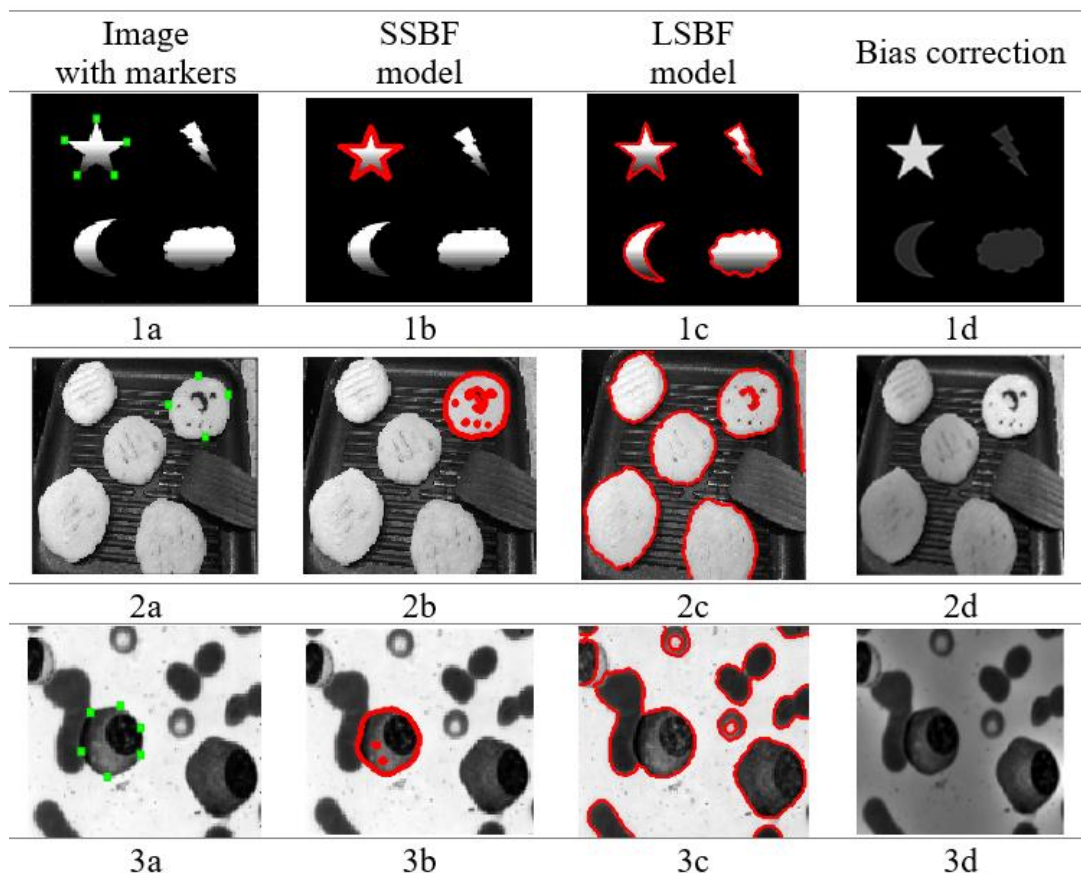


Figure 1. Segmentation results between SSBF model and LSBF model.

Figure 1 demonstrates the segmentation results between the SSBF model (1b-3b) and the LSBF model (1c-3c) in the second and third columns, respectively, with bias correction images in the last column (1d-3d) based on the input images in the first column. The targeted object is indicated by the green marker in the given images (1a-3a).

In this experiment, both models were able to produce the bias correction images. Bias correction images help to homogenize the intensities of the tested images to assist in obtaining accurate segmentation results. As we can observe

from Figure 1, the SSBF model is able to selectively segment the targeted object. However, the LSBF is over segmented and fails to segment the targeted object; instead, the model tries to segment every object in the given input image. Table 2 shows the comparison of the accuracy of the segmentation results between the SSBF model and the LSBF model.

**Table 2.** JSC and DSC values between the SSBF model and the LSBF model.

| Images  | JSC   |       | DSC   |       |
|---------|-------|-------|-------|-------|
|         | SSBF  | LSBF  | SSBF  | LSBF  |
| 1a      | 0.860 | 0.207 | 0.925 | 0.343 |
| 2a      | 0.897 | 0.149 | 0.945 | 0.259 |
| 3a      | 0.845 | 0.200 | 0.916 | 0.333 |
| Average | 0.867 | 0.185 | 0.929 | 0.312 |

Table 2 depicts the JSC and DSC values between the SSBF model and the LSBF model. We can infer that, due to the global segmentation property of LSBF, the accuracy of the segmentation results was affected. As we can see from the table, the average values of JSC and DSC coefficients for the LSBF model were lower than those for the SSBF models. Meanwhile, the SSBF model's average accuracy values surpassed those of the LSBF model, whose average accuracy values are close to 1, indicating good segmentation performance.

#### 4.2. Experiment 2: Comparison of the SSBF Model with the IIS Model

The IIS model by Nguyen, et al. [14] was acknowledged for its reliability in segmenting a particular object in an image [24]. Therefore, in Experiment 2, we are interested in comparing the accuracy of the popular selective segmentation model, the IIS model, with our proposed SSBF model. There were two synthetic images with different levels of intensity inhomogeneity used in this experiment. All test images have dimensions of  $128 \times 128$  pixels. The segmentation results of the SSBF model and the IIS model on inhomogeneous intensities are presented in Figure 2 as follows:

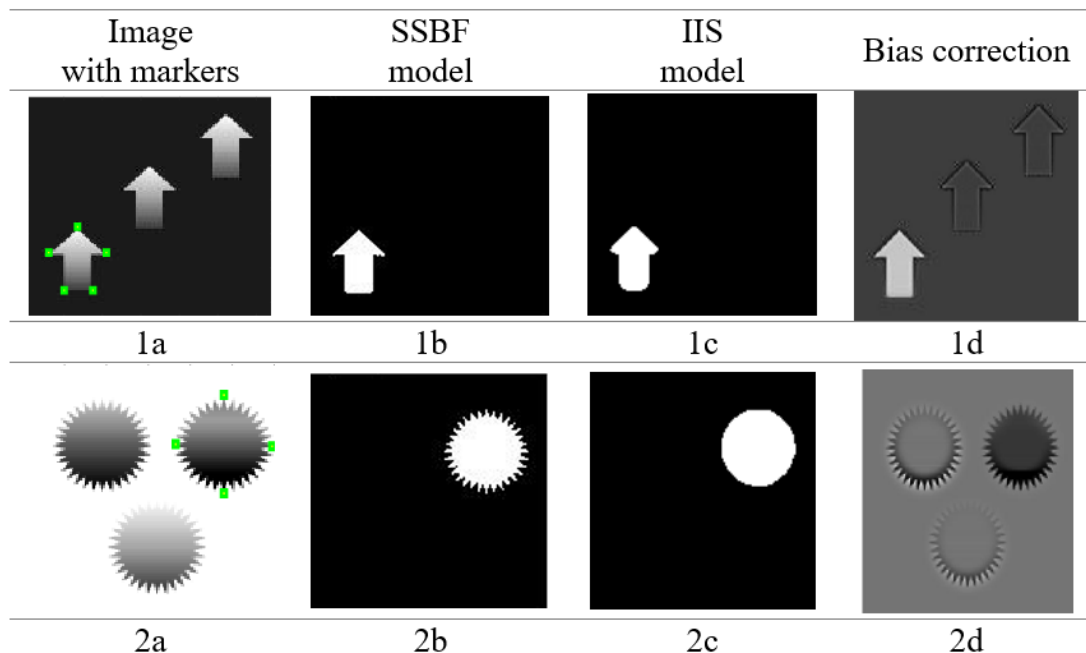


**Figure 2.** Segmentation results between SSBF model and IIS model.

Based on Figure 2, the segmentation results were in binary form to allow for a fair comparison of the outcomes of both models. The IIS model was recognized as having the most promising results when segmenting objects with

intensity inhomogeneity. However, the IIS model has a few drawbacks, such as the fact that it cannot segment images with fine structure. As shown in the figure above, our SSBF model exceeded the IIS model. For both images, the IIS model was unable to neatly segment the irregular region of the targeted object. As a result, the IIS model is unable to partition the targeted object into sophisticated shapes. We also presented the accuracy table of the JSC and DSC coefficients in Table 3.

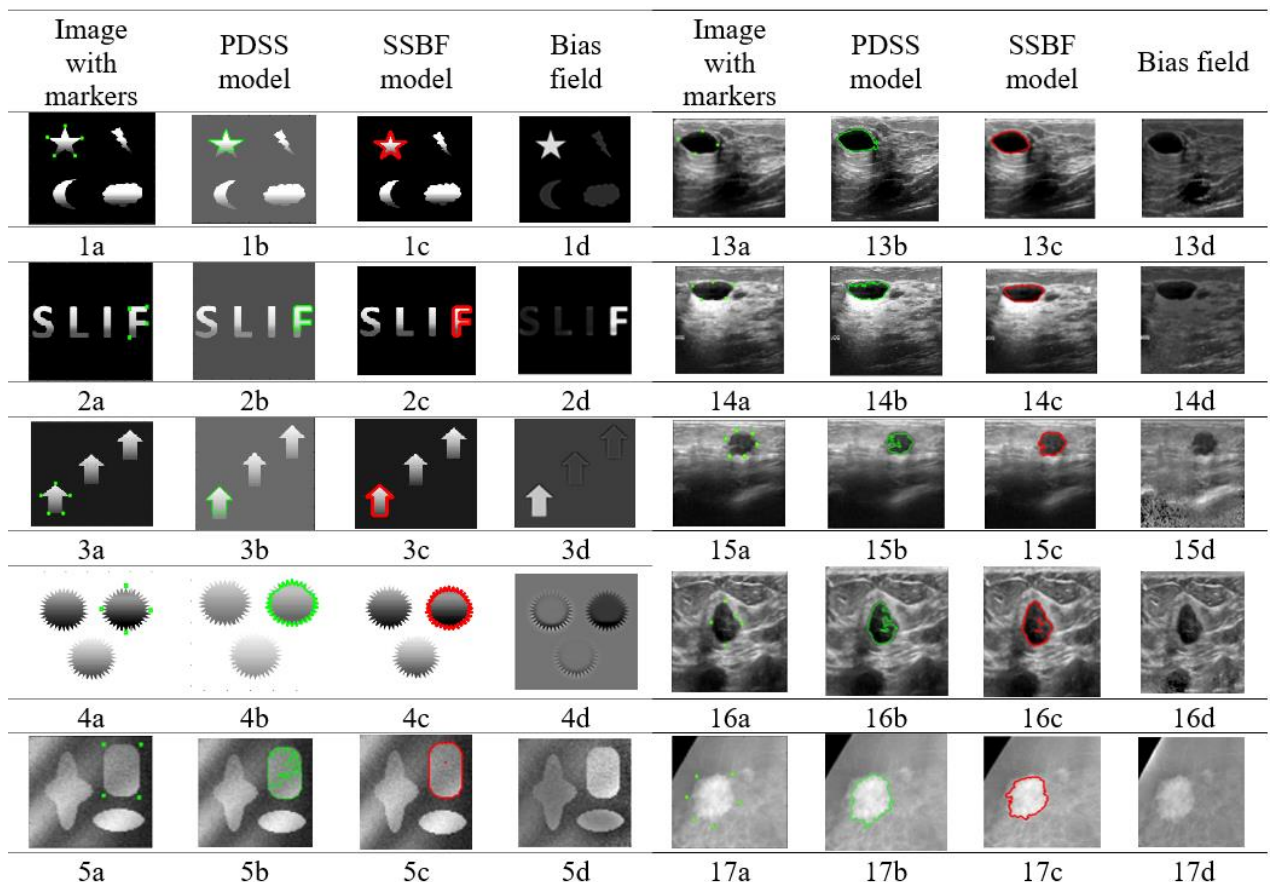
**Table 3.** JSC and DSC values between the SSBF model and the IIS model.

| Image   | JSC   |       | DSC   |       |
|---------|-------|-------|-------|-------|
|         | SSBF  | IIS   | SSBF  | IIS   |
| 1a      | 0.930 | 0.900 | 0.964 | 0.950 |
| 2a      | 0.873 | 0.870 | 0.932 | 0.930 |
| Average | 0.902 | 0.885 | 0.948 | 0.940 |

The average of JSC and DSC values was slightly higher than the IIS model, as indicated in Table 3. Hence, we may conclude that, in terms of segmentation accuracy, the SSBF model is comparable to the IIS model.

#### 4.3. Experiment 3: Comparison of the SSBF Model with the PDSS Model

Next, we compared the proposed SSBF model against the competitor model, the PDSS model, to test their capabilities. All test images have dimensions of  $128 \times 128$  pixels. We set the tolerance (*tol*) and maximum iteration (*maxit*) to 0.005 and 300 respectively, as the stopping criteria. For parameter setting, the range for  $\theta$  and  $\sigma$  were [50,2500] and [1,20] respectively, where the values were, varies depending on the test images. In this experiment, we test the performance of the PDSS model and the SSBF model in segmenting images with intensity inhomogeneity, as demonstrated in Figure 3.



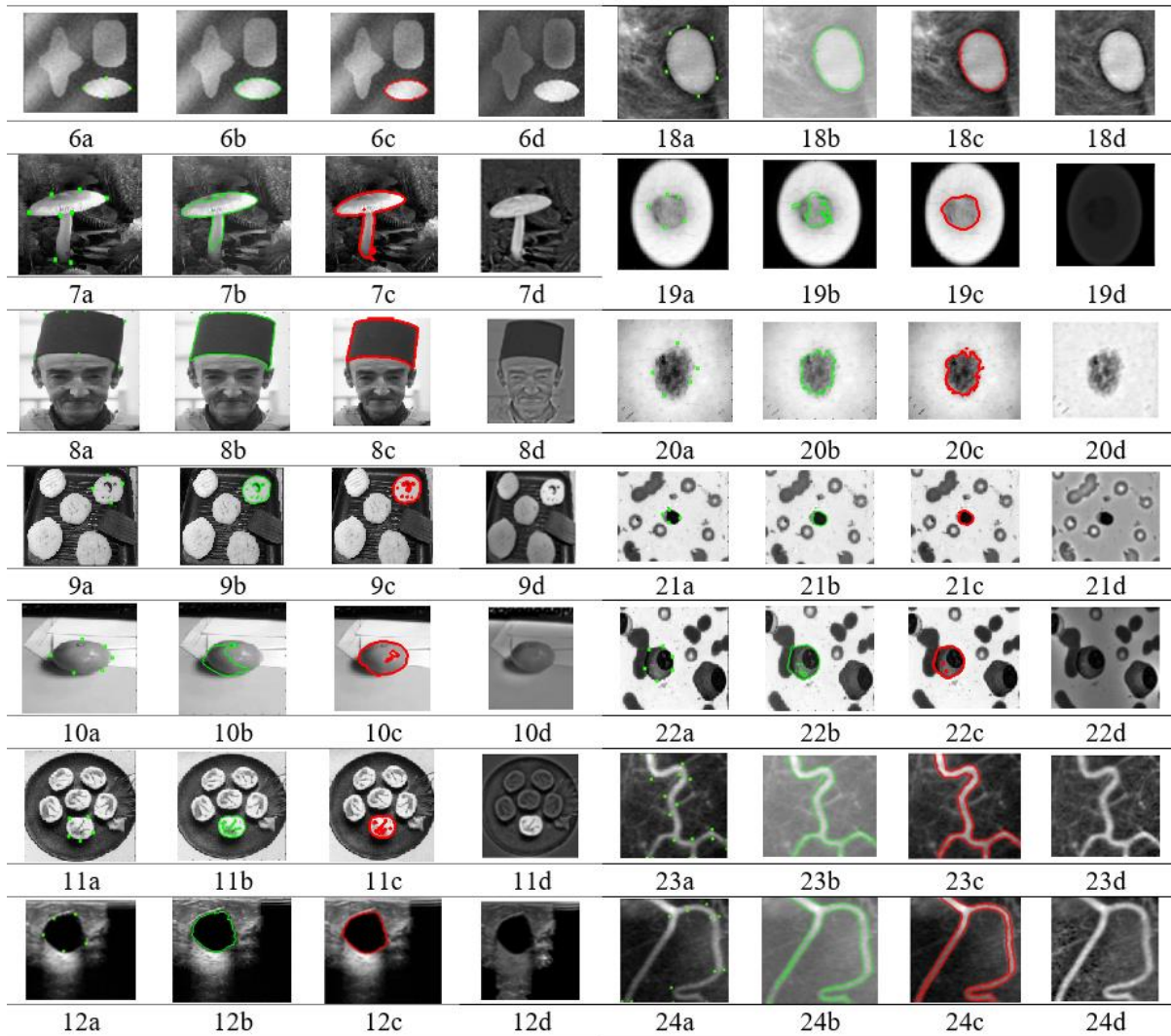


Figure 3. Segmentation results using the SSBF and the PDSS model.

Figure 3 demonstrates the test image with markers used in the first and fifth columns (1a-24a). The second and sixth columns (1b-24b) showed the results delivered by the PDSS model, while the third and seventh columns (1c-24c) demonstrated the results delivered by the SSBF model. The bias-corrected results produced by our SSBF model are shown in the last column (1d-24d). Bias correction images were used in this study to gain an accurate result. As shown in the figure above, our SSBF model was able to segment all the targeted objects highlighted with green markers compared to the PDSS model.

As stated in the previous chapter, the PDSS model was the reformulated version of the CDSS model by Spencer and Chen [10]. The method was defined as an unconstrained minimization problem and significantly uses the Euclidean distance function in its function, which helps to selectively segment the targeted object in the given images. However, the PDSS model is unable to segment intensity inhomogeneity images. For example, in Figure 3 (7b), the PDSS model is unable to segment appropriately due to severe intensity inhomogeneity in the given image. Even though the PDSS model uses the Euclidean distance function to find a specific object, it does not include local intensity information or bias field correction, which are important for separating images with different levels of brightness.

In addition to visual observation, the accuracy of the segmentation results for both models is presented in Table 4.

**Table 4.** JSC and DSC values between the SSBF and the PDSS model.

| Image   | JSC   |       | DSC   |       |
|---------|-------|-------|-------|-------|
|         | PDSS  | SSBF  | PDSS  | SSBF  |
| 1       | 0.722 | 0.860 | 0.838 | 0.925 |
| 2       | 0.733 | 0.869 | 0.846 | 0.930 |
| 3       | 0.773 | 0.930 | 0.872 | 0.964 |
| 4       | 0.836 | 0.873 | 0.911 | 0.932 |
| 5       | 0.839 | 0.988 | 0.912 | 0.994 |
| 6       | 0.933 | 0.964 | 0.966 | 0.982 |
| 7       | 0.831 | 0.974 | 0.907 | 0.987 |
| 8       | 0.915 | 0.928 | 0.956 | 0.963 |
| 9       | 0.826 | 0.897 | 0.905 | 0.945 |
| 10      | 0.403 | 0.846 | 0.574 | 0.917 |
| 11      | 0.579 | 0.716 | 0.733 | 0.835 |
| 12      | 0.886 | 0.934 | 0.939 | 0.965 |
| 13      | 0.842 | 0.878 | 0.914 | 0.935 |
| 14      | 0.789 | 0.803 | 0.882 | 0.891 |
| 15      | 0.576 | 0.776 | 0.731 | 0.874 |
| 16      | 0.598 | 0.735 | 0.749 | 0.848 |
| 17      | 0.806 | 0.809 | 0.892 | 0.894 |
| 18      | 0.869 | 0.898 | 0.930 | 0.946 |
| 19      | 0.455 | 0.843 | 0.626 | 0.915 |
| 20      | 0.632 | 0.677 | 0.774 | 0.808 |
| 21      | 0.667 | 0.677 | 0.799 | 0.807 |
| 22      | 0.828 | 0.845 | 0.906 | 0.916 |
| 23      | 0.781 | 0.885 | 0.877 | 0.939 |
| 24      | 0.700 | 0.787 | 0.823 | 0.881 |
| Average | 0.806 | 0.914 | 0.891 | 0.955 |

Table 4 illustrates the average of JSC and DSC values for the PDSS and SSBF models. The study findings indicate that the mean accuracy values of Jaccard similarity coefficient (JSC) and Dice similarity coefficient (DSC) for the SSBF model in columns three and five were 0.914 and 0.955, respectively. These values were observed to be 13.4% and 7.2% higher than the corresponding values obtained for the PDSS models, respectively. Hence, we can infer that the SSBF model is capable of segmenting the targeted object with intensity inhomogeneity better than the PDSS model in synthetic images.

#### 4.4. Experiment 4: Parameter Sensitivity Analysis

In Experiment 4, the parameter of the SSBF model shall be tested for its sensitivity. We focus on two parameters: the area parameter  $\theta$  and the standard deviation parameter  $\sigma$ . These parameters must be manually adjusted through trial and error to achieve relevant and successful segmentation results.

##### 4.4.1. Results of the SSBF Model with Different Values of Parameter $\theta$

The value of the area parameter  $\theta$  is crucial to enclosing the region of interest since the SSBF model is a selective segmentation model. As indicated in the preceding experiment, our proposed SSBF model chooses an object to be segmented by using the initial green marker set as a foreground marker. It is significant to test whether the SSBF model is sensitive to the area parameter  $\theta$  to enclose the region of interest. The segmentation results with different parameter  $\theta$  values are shown in Figure 4.

Figure 4 illustrates the outcome of the segmentation results using different values parameter  $\theta$ . It shows that when the parameter is too low, the result of the segmented region will be over-segmented resulting in difficulties in interpreting the important information in the image [3]. As we can see, the background tissue of the mammogram image was segmented too due to the small parameter  $\theta$  used. Meanwhile, if the parameter  $\theta$  was too large ( $\theta = 2500$ ), the segmentation of the targeted object would result in an undesirable polygon. Therefore, the optimal value

of parameter for this test image is  $\theta = 40$  as shown in Figure 4. According to Jumaat and Chen [25] and Jumaat and Chen [26], the parameter  $\theta$  must be regulated in order to obtain a successful result from segmentation.

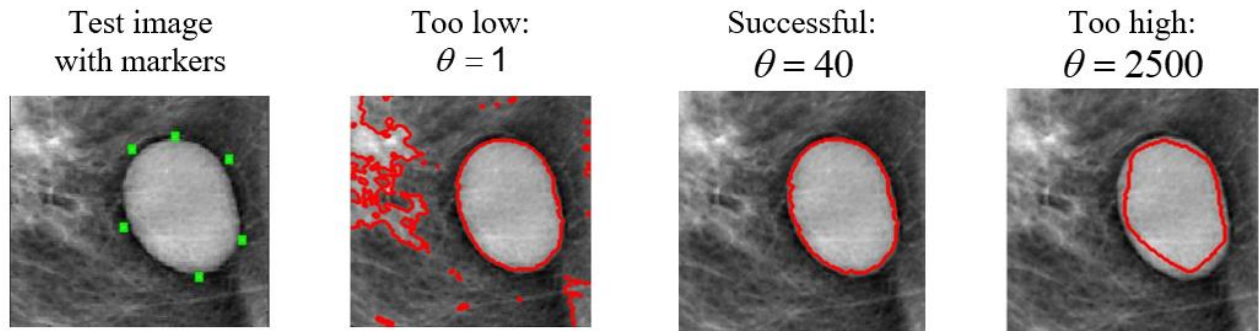


Figure 4. Segmentation results with different values of parameter  $\theta$ .

#### 4.4.2. Results of the SSBF Model with Different Values of Parameter $\sigma$

The standard deviation parameter  $\sigma$  plays an important role in the SSBF model. This parameter  $\sigma$  will control the size of the neighbourhood in the SSBF formulation. Figure 5 demonstrates the segmentation results with different values of the parameter  $\sigma$ .

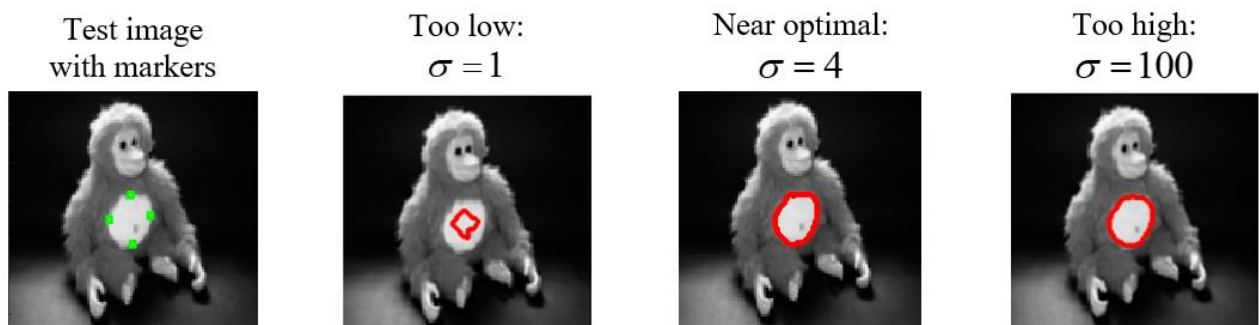


Figure 5. Segmentation results with different values of parameter  $\sigma$  using SSBF model.

According to Figure 5, when a near-optimal value of the parameter  $\sigma$  was used, a better segmentation result was achieved. However, it resulted in unsatisfactory segmentation results if the value of the parameter  $\sigma$  was too small. Note that even if the value of the parameter  $\sigma$  was set to a high value, a better segmentation result was obtained. Table 5 shows the accuracy and efficiency of the SSBF model with different values of parameter  $\sigma$  for segmenting the Monkey's belly.

Table 5. JSC and DSC values for different values of parameter  $\sigma$  using SSBF model.

| Value of parameter $\sigma$ | JSC   | DSC   | Time   |
|-----------------------------|-------|-------|--------|
| 1                           | 0.226 | 0.368 | 15.743 |
| 4                           | 0.974 | 0.987 | 17.800 |
| 100                         | 0.945 | 0.972 | 73.820 |

From Table 5, when  $\sigma = 100$ , the JSC and DSC values were slightly decreased compared to  $\sigma = 4$ . However, it still produces a better result, which is near to the value 1. The average processing time when  $\sigma = 100$  was 73.820 seconds. It was four times slower than  $\sigma = 4$  which 17.800 seconds. By choosing an unsuitable value of the parameter  $\sigma$ , it will lead to unfavourable outcomes. Hence, we may deduce that to achieve better segmentation results, optimum value for the parameter  $\sigma$  is required.

#### 4.5. Limitation of the SSBF Model Compared to the PDSS Model

In this section, we compared the processing time for the proposed SSBF model with the competing selective segmentation model, the PDSS model only. We remarked that since the software the authors [14] provided to implement the IIS model does not have any built-in functions or tools for recording time processing, we were unable to compare the efficiency of the SSBF with the IIS model. Another model that is not considered for the efficiency test is the LSBF model. The LSBF model is a global segmentation type where all the segmentation results fail, as indicated in Experiment 1, so efficiency comparisons with the LSBF model are not significant and were not conducted as well.

Even though the SSBF model outperformed the PDSS model in terms of accuracy, the SSBF model has its limitations in this study. The drawback of this SSBF model is its efficiency; it takes a longer time to process the segmented images. The average processing time in Experiment 3 for the PDSS model is 16.5 seconds, while the proposed SSBF model takes 21.2 seconds. This indicates that the average time taken for the SSBF model to generate the segmentation results was about 5 seconds slower than the PDSS model. This is due to the implementation of bias correction in the SSBF model, which increases the computational complexity of the model and results in slow segmentation processing time.

In addition, the limitations of the SSBF model can be seen in the parameter selection approach. In this model, the parameters  $\theta$  and  $\sigma$  were chosen by trial and error to achieve good segmentation results, which is difficult and time-consuming.

## 5. CONCLUSION

This study employs a selective segmentation model to effectively partition the desired objects inside an image exhibiting intensity inhomogeneity. It was noted that the segmentation tasks posed challenges when applied to intensity inhomogeneity images. Hence, a novel model known as the Selective Segmentation with Bias Field Correction (SSBF) model has been devised. The SSBF model is derived by integrating the PDSS model with the LSBF model. In the new proposed model, the equation involved in minimizing the energy functional of the SSBF model, which is the EL equation, is constructed. Along with that, using the MATLAB software, we have implemented the algorithms. Numerical experiments conducted show that our new model records the highest average accuracy of segmentation compared to the competing models. In addition, the experimental results show that appropriate values of  $\theta$  and  $\sigma$  are needed to acquire better segmentation results as the SSBF model is sensitive to parameter values. The parameters were set manually by trial and error. As a result, we can conclude that the SSBF model successfully segmented the region of interest with good segmentation accuracy in images with intensity inhomogeneity. Nevertheless, the SSBF model has a limitation in this study. As expected, the drawback of the SSBF model is its efficiency. According to the experiment conducted, the SSBF model takes longer to process compared to the PDSS model. In the future, the SSBF model can be extended to a 3-D formulation.

**Funding:** This study received no specific financial support.

**Institutional Review Board Statement:** Not applicable.

**Transparency:** The authors state that the manuscript is honest, truthful, and transparent, that no key aspects of the investigation have been omitted, and that any differences from the study as planned have been clarified. This study followed all writing ethics.

**Competing Interests:** The authors declare that they have no competing interests.

**Authors' Contributions:** Conceptualization and methodology, N.A.S.R. and A.K.J.; formal analysis, N.A.S.R.; resources, A.K.J.; writing, review and editing, N.A.S.R., A.K.J., M.A.M., M.F.L., and N.N.A.R.; supervision, A.K.J., M.A.M., M.F.L., and N.N.A.R. All authors have read and agreed to the published version of the manuscript.

**Acknowledgement:** The APC was funded by Pembiayaan Yuran Penerbitan Artikel, Tabung Dana Kecemerlangan Pendidikan, Universiti Teknologi MARA, Malaysia.

## REFERENCES

- [1] S. Saifullah, "Segmentation for embryonated egg images detection using the K-Means algorithm in image processing " presented at the In 2020 5th International Conference on Informatics and Computing, ICIC 2020, 2020.
- [2] J. Zhang, J. Qi, Z. Zheng, and L. Sun, "A robust image segmentation framework based on total variation spectral transform," *Pattern Recognition Letters*, vol. 153, pp. 159-167, 2022. <https://doi.org/10.1016/j.patrec.2021.12.001>
- [3] A. K. Jumaat, W. E. Z. W. A. Rahman, A. Ibrahim, and R. Mahmud, "Segmentation and characterization of masses in breast ultrasound images using active contour," in *In 2011 IEEE International Conference on Signal and Image Processing Applications (ICSIPA)*, 2011, pp. 404-409.
- [4] S. S. Yasiran, "Comparison between GVF snake and ED snake in segmenting microcalcifications," presented at the In ICCAIE 2011 - 2011 IEEE Conference on Computer Applications Ind Electron, 2011.
- [5] S. S. Yasiran *et al.*, "Microcalcifications segmentation using three edge detection techniques," presented at the In 2012 IEEE International Conference on Electronics Design, Systems and Applications (ICEDSA), IEEE, 2012.
- [6] A. K. Jumaat, "Performance comparison of Canny and Sobel edge detectors on Balloon Snake in segmenting masses," presented at the In 2014 International Conference on Computer and Information Sciences (ICCOINS), 2014.
- [7] B. Huang, Z. Pan, H. Yang, and L. Bai, "Variational level set method for image segmentation with simplex constraint of landmarks," *Signal Processing: Image Communication*, vol. 82, p. 115745, 2020.
- [8] T. F. Chan and L. A. Vese, "Active contours without edges," *IEEE Transactions on Image Processing*, vol. 10, no. 2, pp. 266-277, 2001.
- [9] D. Mumford and J. Shah, "Optimal approximations by piecewise smooth functions and associated variational problems," *Communications on Pure and Applied Mathematics*, vol. 42, no. 5, pp. 577-685, 1989.
- [10] J. Spencer and K. Chen, "A convex and selective variational model for image segmentation," *Communications in Mathematical Sciences*, vol. 13, no. 6, pp. 1453-1472, 2015. <https://doi.org/10.4310/cms.2015.v13.n6.a5>
- [11] A. K. Jumaat and K. Chen, "A reformulated convex and selective variational image segmentation model and its fast multilevel algorithm," *Numerical Mathematics*, vol. 12, no. 2, pp. 403-437, 2019. <https://doi.org/10.4208/nmtma.0a-2017-0143>
- [12] C. Li, R. Huang, Z. Ding, J. C. Gatenby, D. N. Metaxas, and J. C. Gore, "A level set method for image segmentation in the presence of intensity inhomogeneities with application to MRI," *IEEE Transactions on Image Processing*, vol. 20, no. 7, pp. 2007-2016, 2011. <https://doi.org/10.1109/tip.2011.2146190>
- [13] T. Ivanovska *et al.*, "An efficient level set method for simultaneous intensity inhomogeneity correction and segmentation of MR images," *Computerized Medical Imaging and Graphics*, vol. 48, pp. 9-20, 2016. <https://doi.org/10.1016/j.compmedimag.2015.11.005>
- [14] T. N. A. Nguyen, J. Cai, J. Zhang, and J. Zheng, "Robust interactive image segmentation using convex active contours," *IEEE Transactions on Image Processing*, vol. 21, no. 8, pp. 3734-3743, 2012. <https://doi.org/10.1109/tip.2012.2191566>
- [15] M.-L. Huang and Y.-Z. Wu, "Semantic segmentation of pancreatic medical images by using convolutional neural network," *Biomedical Signal Processing and Control*, vol. 73, p. 103458, 2022. <https://doi.org/10.1016/j.bspc.2021.103458>
- [16] S. Lankton and A. Tannenbaum, "Localizing region-based active contours," *IEEE Transactions on Image Processing*, vol. 17, no. 11, pp. 2029-2039, 2008. <https://doi.org/10.1109/tip.2008.2004611>
- [17] D. Martin, C. Fowlkes, D. Tal, and J. Malik, "A database of human segmented natural images and its application to evaluating segmentation algorithms and measuring ecological statistics," in *In Proceedings of the IEEE International Conference on Computer Vision*, 2001, vol. 2, pp. 416-423.
- [18] M. Y. Chen, "Automatic Chinese food identification and quantity estimation," *SIGGRAPH Asia 2012 Technical Briefs, SA*, vol. 1, no. 212, pp. 3-6, 2012.
- [19] J. Li, C. Xia, and X. Chen, "A benchmark dataset and saliency-guided stacked autoencoders for video-based salient object detection," *IEEE Transactions on Image Processing*, vol. 27, no. 1, pp. 349-364, 2017. <https://doi.org/10.1109/tip.2017.2762594>

- [20] I. C. Moreira, I. Amaral, I. Domingues, A. Cardoso, M. J. Cardoso, and J. S. Cardoso, "Inbreast: Toward a full-field digital mammographic database," *Academic Radiology*, vol. 19, no. 2, pp. 236-248, 2012.
- [21] A. Rodtook, K. Kirimasthong, W. Lohitvisate, and S. S. Makhanov, "Automatic initialization of active contours and level set method in ultrasound images of breast abnormalities," *Pattern Recognition*, vol. 79, pp. 172-182, 2018. <https://doi.org/10.1016/j.patcog.2018.01.032>
- [22] Ismahan, "Microscopic bone marrow images dataset", Retrieved: <https://www.kaggle.com/datasets/fanouna/microscopic-bone-marrow-images>. [Accessed 27 November 2022], 2020.
- [23] N. C. Codella *et al.*, "Skin lesion analysis toward melanoma detection: A challenge at the 2017 international symposium on biomedical imaging (ISBI), hosted by the international skin imaging collaboration (ISIC)," presented at the In 2018 IEEE 15th International Symposium on Biomedical Imaging (ISBI 2018), IEEE, 2018.
- [24] N. A. S. M. Ghani, A. K. Jumaat, R. Mahmud, M. A. Maasar, F. A. Zulkifle, and A. M. Jasin, "Breast abnormality boundary extraction in mammography image using variational level set and self-organizing map (SOM)," *Mathematics*, vol. 11, no. 4, p. 976, 2023. <https://doi.org/10.3390/math11040976>
- [25] A. K. Jumaat and K. Chen, "An optimization-based multilevel algorithm for variational image segmentation models," *Electronic Transactions on Numerical Analysis*, vol. 46, pp. 474-504, 2017.
- [26] A. K. Jumaat and K. Chen, "Three-dimensional convex and selective variational image segmentation model," *Malaysian Journal of Mathematical Sciences*, vol. 14, no. 3, pp. 437-450, 2020.

*Views and opinions expressed in this article are the views and opinions of the author(s). Review of Computer Engineering Research shall not be responsible or answerable for any loss, damage or liability etc. caused in relation to/arising out of the use of the content.*